Senolytics reduce coronavirus-related mortality in old mice

Christina D. Camell[1]†, Matthew J. Yousefzadeh[1]†, Yi Zhu[2,3]†, Larissa G. P. Langhi Prata[2]†, Matthew A. Huggins[4], Mark Pierson[4], Lei Zhang[1], Ryan D. O'Kelly[1], Tamar Pirtskhalava[2], Pengcheng Xun[5], Keisuke Ejima[5], Ailing Xue[2], Utkarsh Tripathi[2], Jair Machado Espindola-Netto[2], Nino Giorgadze[2], Elizabeth J. Atkinson[2,6], Christina L. Inman[2], Kurt O. Johnson[2], Stephanie H. Cholensky[1], Timothy W. Carlson[5], Nathan K. LeBrasseur[2,3], Sundeep Khosla[2,7], M. Gerard O'Sullivan[8,9], David B. Allison[5], Stephen C. Jameson[4], Alexander Meves[10], Ming Li[10], Y. S. Prakash[3,11], Sergio E. Chiarella[12], Sara E. Hamilton[4]*, Tamara Tchkonia[2,3]*, Laura J. Niedernhofer[1]*, James L. Kirkland[2,13]*, Paul D. Robbins[1]*

[1]Institute on the Biology of Aging and Metabolism, Department of Biochemistry, Molecular Biology and Biophysics, University of Minnesota, Minneapolis, MN, USA. [2]Robert and Arlene Kogod Center on Aging, Mayo Clinic, Rochester, MN, USA. [3]Department of Physiology and Biomedical Engineering, Mayo Clinic, Rochester, MN, USA. [4]Department of Laboratory Medicine and Pathology and Center of Immunology, University of Minnesota, Minneapolis, MN, USA. [5]Department of Epidemiology & Biostatistics, School of Public Health, Indiana University-Bloomington, Bloomington, IN, USA. [6]Division of Biomedical Statistics and Informatics, Department of Health Sciences Research, Mayo Clinic, Rochester, MN, USA. [7]Division of Endocrinology, Department of Medicine, Mayo Clinic, Rochester, MN, USA. [8]Masonic Cancer Center Comparative Pathology Shared Resource, University of Minnesota, St. Paul, MN, USA. [9]Department of Veterinary Population Medicine, University of Minnesota, St. Paul, MN, USA. [10]Department of Dermatology, Mayo Clinic, Rochester, MN, USA. [11]Department of Anesthesiology and Perioperative Medicine, Mayo Clinic, Rochester, MN, USA. [12]Division of Allergic Diseases, Department of Medicine, Mayo Clinic, Rochester, MN, USA. [13]Division of General Internal Medicine, Department of Medicine, Mayo Clinic, Rochester, MN, USA.

†These authors contributed equally to this work.

*Corresponding author. Email: probbins@umn.edu (P.D.R.); kirkland.james@mayo.edu (J.L.K.); lniedern@umn.edu (L.J.N.); tchkonia.tamar@mayo.edu (T.T.); hamil062@umn.edu (S.E.H.)

The COVID-19 pandemic has revealed the pronounced vulnerability of the elderly and chronically-ill to SARS-CoV-2-induced morbidity and mortality. Cellular senescence contributes to inflammation, multiple chronic diseases, and age-related dysfunction, but effects on responses to viral infection are unclear. Here, we demonstrate that senescent cells (SnC) become hyper-inflammatory in response to pathogen-associated molecular patterns (PAMPs), including SARS-CoV-2 Spike protein-1, increasing expression of viral entry proteins and reducing anti-viral gene expression in non-SnCs through a paracrine mechanism. Old mice acutely infected with pathogens that included a SARS-CoV-2-related mouse β-coronavirus experienced increased senescence and inflammation with nearly 100% mortality. Targeting SnCs using senolytic drugs before or after pathogen exposure significantly reduced mortality, cellular senescence, and inflammatory markers and increased anti-viral antibodies. Thus, reducing the SnC burden in diseased or aged individuals should enhance resilience and reduce mortality following viral infection, including SARS-CoV-2.

Old age is the greatest risk factor by orders of magnitude for most chronic diseases including cancers, diabetes, cardiovascular disease, and Alzheimer's disease. Aging also predisposes to geriatric syndromes and loss of physical resilience. The current COVID-19 pandemic has illuminated the exquisite vulnerability of the elderly and those with underlying geriatric syndromes to increased SARS-CoV-2-mediated mortality (*1–5*). Thus, approaches to extend health span and enhance physical resilience could reduce the rate of mortality in elderly COVID-19 patients.

Cellular senescence has emerged as one of the mechanisms that drives aging and age-related diseases that is most tractable to therapeutically target (*6, 7*). Senescence is a cell fate elicited in response to external and internal cellular stress signals, established through transcription factor cascades that can include $p16^{INK4a}$/retinoblastoma protein and/or $p53/p21^{CIP1}$, which cause extensive changes in gene expression, histone modifications, organelle function, elevated protein production, and profound morphologic and metabolic shifts (*8, 9*). A significant fraction of senescent cells (SnC) release inflammatory factors, chemokines, growth factors, proteases, bioactive lipids, extracellular vesicles, and pro-coagulant factors, termed the senescence-associated secretory phenotype or SASP (*6*).

Senescence is a robust tumor suppressor mechanism, with the SASP acting as a chemoattractant stimulating immune cell-mediated clearance of senescent and neighboring cells. However, with advancing age and many chronic diseases,

First release: 8 June 2021
www.sciencemag.org
(*Page numbers not final at time of first release*)   1

SnC accumulate in most tissues, presumably due to inefficient SnC removal by the immune system and resistance to cell death. This accumulation drives chronic sterile inflammation, which in turn drives loss of resilience and predisposition to many diseases (*10*). SnC can interfere with the immune system and the ability of immune cells to remove them. For example, the SASP factors, IL-6, MCP-1, and CCL11, alter myeloid cell migration, IP10/CXCL10 depletes critical T lymphocyte subsets, and matrix metalloproteinases cleave FAS ligand and other immune system regulators (*11*). The SASP can drive fibrosis (*11*). SnC have been demonstrated to play a causal role in aging and age-related diseases in preclinical models. Transplanting SnC into young mice causes an accelerated aging-like state, while genetic or pharmacologic selective killing of SnC attenuates disease, improves physical function, and delays all-cause mortality in older mice (*12–14*). Importantly, factors that are common components of the SASP are linked to prolonged disease, hyperinflammation/cytokine storm/acute respiratory distress syndrome (ARDS), myocarditis with troponin leak, T cell deficiencies, clotting, delirium, and multi-organ failure in SARS-CoV2 patients (*15*). Also, a signature of the SASP factors IL-6, IL-10, and IP-10 in COVID-19 patients appears to predict clinical progression (*16*). However, it is not known whether SnC and their pro-inflammatory SASP contribute to the increased mortality observed in the elderly and chronically-diseased following infection.

Initially, to determine if SnC have an altered response to pathogen exposure compared to healthy cells, we treated irradiation-induced senescent human pre-adipocytes and non-senescent cells with the pathogen-associated molecular pattern (PAMP) factor lipopolysaccharide (LPS). LPS stimulated expression of *IL1α*, *IL1β*, *IL6*, *MCP1*, and *PAI2* in non-SnC (Fig. 1A, fig. S1, and table S1) but did not significantly alter levels of *p16^INKa* or *p21^CIP1*. Expression of these SASP factors, as well as *IL10* and *PAI1* were all significantly increased by LPS in SnC relative to untreated SnC and relative to LPS-treated non-SnC, suggesting that PAMPs exacerbate the SASP and SnC can amplify the inflammatory response to PAMPs. To determine if a similar effect occurs in vivo, young and aged wild-type (WT) mice were challenged with LPS. Senescence and SASP markers were measured 24 hours post-treatment. Although expression of the senescence markers, *p16^Ink4a* and *p21^Cip1*, was not affected at this early time point, LPS exposure stimulated a significant increase in expression of *Il1α*, *Il1β*, *Il6*, *Il10*, *Mcp1*, *Tnfα*, *Pai1*, and *Pai2* in liver (Fig. 1B) and kidney (fig. S2) of aged compared to young mice. Furthermore, LPS challenge significantly increased levels of the SASP factors IL-6, MCP-1, and TNFα in the serum of old mice (Fig. 1C). To confirm the effect of LPS on aged mice with an increased SnC burden, we also treated progeroid *Ercc1^-/Δ* mice (fig. S3), which express high levels of senescence and SASP markers in the same tissues and to the same extent as occurs in wild-type mice albeit much earlier in life (*17*), acutely with LPS. Senescence and SASP markers were measured 24 hours post-treatment. Although expression of senescence markers *p16^Ink4a* and *p21^Cip1* was not affected at this early time point, LPS significantly increased expression of SASP factors (*Il1α*, *Il1β*, *Il6*, *Tnfα*, and *Mcp1*) in kidney and liver of the progeroid mice relative to age-matched wild-type controls (fig. S3) and significantly increased levels of circulating IL-6 and MCP-1 (fig. S3). Based on these results, we hypothesized that SnCs exposed to pathogen-associated signals contribute to hyper-inflammation and cytokine storm following infection with pathogens.

Senescent cells have an altered response to SARS-CoV-2 spike protein

Viral entry through cell surface receptors and dampening of host anti-viral gene expression are critical steps in successful infections and virus propagation (*18*). The spike 1 (S1) glycoprotein of SARS-CoV-2, antibodies against which are currently being tested in clinical trials (NCT04425629), mediates entry into host cells through binding to angiotensin-converting enzyme 2 (ACE-2), resulting in elevated NF-κB signaling and inflammatory cytokine production (*19*, *20*). Endothelial cells can be infected directly by SARS-CoV-2, leading to amplification of inflammation with significant changes in endothelial morphology and disruption of intercellular junctions (*21*).

To address specifically how the SARS-CoV-2 PAMPs impact SnC, senescent human kidney endothelial cells (fig. S4) were treated with pyrogen-free recombinant S1 protein. Exposing endothelial SnC to S1 for 24 hours significantly increased secretion of the majority of endothelial SASP factors measured in the conditioned media (composite score p < 0.0089 comparing SnC to non-SnC: Fig. 2A and table S2). Similar, albeit less dramatic, results were obtained using kidney endothelial cells in which senescence was induced by replication rather than radiation (fig. S5 and table S3). In addition, treatment of human subcutaneous adipocyte progenitor SnCs with S1 increased expression of the key pre-adipocyte SASP factors, IL1α and IL1β, at the mRNA level (fig. S6). Consistent with the LPS data, these data suggest that S1 is a PAMP that can trigger a hyper-inflammatory state in SnC, possibly through stimulation of a TLR (*22*, *23*), with the inflammatory profile differing among types of SnC.

Inflammatory SASP factors contribute to clearing pathogens. However, certain inflammatory/SASP factors released by senescent human lung cell types, including IL-1α, IL-1β, IL-6, MCP-1, TNFα and MMP-1, are central to the pathological cytokine storm seen in some COVID-19 patients (*4*, *5*, *24–33*). Initially, to determine if the SASP impacts the response of human endothelial cells to pathogen exposure, non-senescent

primary kidney endothelial cells were exposed to conditioned media (CM) from SnC or non-SnC (Fig. 2B). The CM from SnC endothelial cells significantly reduced expression of the key viral defense genes *IFITM2* and *IFITM3* (Fig. 2C). IL-1α is a natural pyrogen as well as a master up-stream regulator of the senescence-associated IL-6/IL-8 cytokine network (*34*). It is elevated in COVID-19 patients (*35*), increased in SnC treated with S1 (fig. S6), and increased in LPS-treated mice (Fig. 1B and figs. S2 and S3). Directly treating non-senescent primary human endothelial cells with IL-1α significantly reduced expression of *IFITM2* and *IFITM3* (Fig. 2D). Suppressing the SASP factors IL-18, PAI-1, and IL-1α, by pretreating the CM from SnC with neutralizing antibodies against these proteins partially restored *IFITM2* and *IFITM3* expression (Fig. 2C). These data support the conclusion that the SASP from pre-existing SnC could exacerbate SARS-CoV-2 infection of non-senescent human endothelial cells.

Next, we examined the impact of the SASP on human lung epithelial cells, another target cell type in COVID-19. Treating non-senescent primary human lung epithelial cells with CM from senescent human preadipocytes, kidney endothelial cells, or human umbilical vein endothelial cells (HUVECs) significantly increased expression of the SARS-CoV-2 viral entry genes *ACE2* and *TMPRSS2* (Fig. 2E). Similarly, treating non-senescent human primary kidney endothelial cells with CM from SnC induced expression of *TMPRSS2* (Fig. 2E). Adding neutralizing antibodies against IL-1α to the CM from SnC kidney endothelial cells reduced expression of *TMPRSS2* while anti-IL-18 did not (Fig. 2F). Treating non-senescent human primary endothelial cells directly with IL-1α increased *TMPRSS2* expression five-fold (Fig. 2F) and IL-1α treatment of non-senescent human lung epithelial cells increased both *ACE2* and *TMPRSS2* expression 2-fold (fig. S7A). Treating non-senescent human kidney endothelial cells with IL-1α also significantly increased expression of *IL6*, *IL8*, *IP10*, and *MCP1* (fig. S7B). In addition, although *ACE2* and *TMPRSS2* were not up-regulated in senescent human pre-adipocytes (fig. S7C) in which these genes are not normally expressed, *TMPRSS2* was up-regulated in senescent human endothelial cells (fig. S7D). Consistent with these in vitro results, in healthy human lung tissue resected from five elderly patients for clinical indications of focal, non-infectious causes, there were more TMPRSS2+ cells adjacent to p16INK4a+ cells as detected by immunofluorescence, with the abundance of p16INK4a+ cells correlating with TMPRSS2+ cell abundance (Fig. 2, G and H). Collectively, these data further support the conclusion that SnC could promote SARS-CoV-2 pathogenesis by decreasing viral defenses and increasing expression of viral entry proteins in neighboring non-SnCs through amplified secretion of SASP factors.

Old mice are hypersensitive to pathogen exposure, including β-coronavirus infection

To investigate the role of SnC in driving adverse outcomes upon infection in vivo, we exploited an experimental paradigm developed to study the response of laboratory (specified-pathogen free; SPF) mice to infection with common murine microbes, creating what is termed a "normal microbial experience" (NME) (*36–38*). Experimental mice are exposed to pathogens via co-housing with pet-store mice or through exposure to their dirty bedding. NME exposure for many months rarely compromises the viability of young mice [89% survival across all experiments; Fig. 3A and (*36–38*)]. In contrast, exposing old mice (20+ months of age) to the same NME rapidly caused nearly 100% lethality in <2 weeks and in both sexes (Fig. 3A and fig. S8A). In mice euthanized on day 6-7 following NME exposure, expression of senescence markers (*p21^{Cip1}* and *p16^{Ink4a}*) and SASP factors (*Il6*, *Mcp1*, and *Tnfα*) in liver, kidney, and to a lesser extent, in lung were increased in old NME mice compared to old SPF, young SPF, or young NME mice (Fig. 3B). In addition, there was an increase in infiltration of CD45+ cells into the liver by day 6-7 following NME exposure in both young and aged mice (fig. S8B). Importantly, the percent of infiltrating immune cells was significantly higher in aged mice than in young animals. These results are consistent with spread of senescence and inflammation following pathogen exposure. In addition, there was a significant increase in SASP-related inflammatory cytokines (IL-6, IL-10, EOTAXIN/CCL11, and TNFα) in the serum of old NME mice compared to young NME mice (Fig. 3C), consistent with pre-existing SnC creating an environment that contributes to hyperinflammation upon infection.

Several viruses were detected in saliva and fecal pellets from the NME mice a week after exposure to pet store mice, including the β-coronavirus mouse hepatitis virus (MHV), a virus in the same family as SARS-CoV-1&2 (table S4). However, by day 11, when the majority of old mice had succumbed to infection, NME mice were serologically positive for MHV, but not the other pathogens carried by pet store mice (Fig. 3D). Histopathology indicated that old, but not young mice had evidence of active MHV infection manifested as multifocal necrotizing hepatitis and the presence of MHV-specific syncytial cells within areas of necrosis (Fig. 3E). In addition, MHV-induced syncytial cells were observed among epithelial cells in the small and large intestines of aged mice (fig. S8C). These findings are consistent with active infection in aged animals, in contrast to rapid clearance in the young animals.

To determine whether MHV infection contributes to NME-mediated mortality in old mice, young and old mice were directly infected with a sublethal dose of MHV (strain A59) prior to NME exposure (Fig. 3F). Old mice challenged with MHV generated a reduced antibody response compared

to young mice (Fig. 3F). However, MHV immunization prevented death of the old mice following NME exposure although the animals were infected with multiple other viruses (table S5), while naïve, old mice succumbed (Fig. 3G). This provides compelling evidence that the β-coronavirus MHV is the primary driver of mortality in old mice in the NME paradigm.

Senolytics reduce senescence, inflammation, and mortality following pathogen exposure

To determine if drugs that induce apoptosis specifically of SnC, termed senolytics, reduce the mortality of old mice acutely infected with pathogens, we tested Fisetin, a natural flavonoid found in many fruits and vegetables (*39*, *40*) that we established as senolytic (*14*, *41*). Fisetin improves tissue homeostasis, reverses age-related tissue damage, and extends median lifespan of mice, even when administered late in life, with no observable adverse effects (*14*, *41*).

Old mice were exposed to NME for 1 week starting on day 0 and were then treated with 20 mg/kg Fisetin via oral gavage on days 3, 4, and 5 and 10, 11, and 12 following pathogen exposure (Fig. 4A), with no evidence of adverse effects. In between Fisetin dosing, the mice were on a maintenance dose of Fisetin (500 ppm fisetin in chow *ad libitum*). Consistent with our previous results (Fig. 3A), 100% of the old mice in the vehicle control groups died within 2 weeks (Fig. 4B sexes combined and S9A graphed by sex). However, 64% of the Fisetin-treated male mice and 22% of the female mice survived long-term with a significant extension of overall lifespan for both sexes. Whether there is a true sex difference in the effect of Fisetin on survival needs to be explored further since the ages of the old male and female mice were not identical.

Notably, on day 11 post-NME, relative levels of anti-MHV antibodies were dramatically lower in the old than young mice (Fig. 4C), consistent with the premature death of the old mice. However, in old mice treated with Fisetin, antibodies against MHV were increased to youthful levels by day 16. All mice exposed to NME were confirmed MHV-positive by RT-PCR at 8 days post-exposure (Fig. 4D). Interestingly, the old mice had significantly more viral mRNA than young mice (Fig. 4D), consistent with impaired immune responses in aged organisms (Fig. 3F) and impaired viral defenses due to senescent cells (Fig. 2C). However, a short duration of Fisetin treatment initiated 3 days after NME exposure tended to reduce the viral mRNA burden in old mice (Fig. 4D; p = 0.09).

To evaluate how Fisetin mediates its protective effects on NME-induced mortality in aged mice, we measured senescence and SASP markers prior to death. SnC markers (*p16^{Ink4a}* or *p21^{Cip1}*) were reduced in the liver, kidney, lung, and spleen of the old Fisetin-treated NME mice compared to old mice receiving vehicle only (Fig. 4E). Furthermore, expression of

multiple SASP inflammatory factors, including *Ifnγ*, *Il1α*, *Il1β*, *Il6*, *Il17*, *Tnfα*, *Cxcl1*, *Cxcl2*, *Cxcl10*, *Mcp1*, *Mip1*, *Pai1*, *Pai2*, *Il2*, and *Il7* was reduced to varying extents in the same tissues (Fig. 4F and fig. S9B). Similarly, the levels of circulating IL-1β, IL-6, MCP-1, and TNFα were reduced following Fisetin treatment (Fig. 4G). Thus, although the old mice were MHV-infected, Fisetin reduced senescence, the SASP, and inflammation post-infection and prolonged survival, enabling an improved antibody response to the virus.

Senolysis contributes to improved outcomes in old mice exposed to pathogens

To determine if the mechanism of action of Fisetin in suppressing adverse outcomes upon viral infection includes senolysis, two approaches were taken. First, *INK-ATTAC* mice were studied under NME conditions to enable genetic ablation of *p16^{Ink4a}*-expressing SnC (*42*). *INK-ATTAC* mice express a caspase 8-FKBP fusion protein, *ATTAC* (*43*), from the *p16^{Ink4a}* promoter. Old *INK-ATTAC* mice (>24 months) were treated with AP20187 to drive dimerization of FKBP, activation of caspase-8, and apoptosis of *p16^{Ink4a}*-expressing cells (3 days per week × 2 weeks), prior to exposure to NME and then weekly post-NME (Fig. 5A). Both control and AP20187-treated mice were positive for MHV RNA at day 8 post-NME exposure (Fig. 5B). AP20187 treatment reduced the expression of the SnC markers, *p16^{Ink4a}* and *p21^{Cip-1}*, and *eGFP* expression, which is also driven by the *p16^{Ink4a}* promoter in *INK-ATTAC* mice following NME exposure (Fig. 5C), as well as certain inflammatory/SASP genes in kidney, liver, brain, pancreas, and/or colon (fig. S10). AP20187 treatment significantly delayed NME-induced mortality in both male and female aged mice (Fig. 5D and fig. S10A), providing evidence that senolysis improves outcomes in aged organisms acutely exposed to pathogens. The level of MHV RNA also trended down following AP20187 treatment (Fig. 5B), consistent with the results with Fisetin treatment.

Second, we tested a different well-established senolytic cocktail, Dasatinib plus Quercetin, D+Q (*12*, *13*), and directly compared it to Fisetin in the same survival experiment. D+Q or Fisetin was administered to aged female mice at days 3 and 4 and 11 and 12 following initiation of NME (Fig. 5E). As expected, while 100% of the old, vehicle-treated mice succumbed to infection, ~50% of the old mice treated with D+Q or Fisetin survived (Fig. 5E). The similarity in survival curves between the two treatment groups is remarkable. This combination of genetic and pharmacologic studies provides strong support for the conclusion that clearing SnC in old organisms contributes to improved outcomes upon acute exposure to viral pathogens.

Finally, to determine if pretreating old mice with Fisetin prior to infection could prevent adverse outcomes, old WT mice were treated with a single round of high dose Fisetin

(20 mg/kg/day for two consecutive days beginning three days prior to NME exposure), followed by low dose Fisetin following infection (fig. S11A). This suppressed mortality in both male and female mice by 40% (fig. S11, A and B). Additionally, anti-MHV antibodies were detected in Fisetin-treated mice on days 16 and 21 (fig. S11C), a time by which all vehicle-treated old mice had died (fig. S11A). To evaluate whether a shorter regimen of senolytic therapy could improve outcomes in old NME mice, animals were given two doses of Fisetin after NME exposure once (days 3 and 4; Fig. 5F) or twice (days 3,4 and 10,11; Fig. 5G). These short course treatments, in the absence of continuous exposure to Fisetin via chow, were sufficient to delay mortality significantly (Fig. 5, F and G). Since Fisetin has an elimination half-life of less than 5 hours (*44*), these data are consistent with a "hit and run" mechanism, whereby Fisetin is acting as a senolytic, reducing overall SnC burden, rather than being required to be present constantly to engage with a molecular target to confer benefit. The data also reveal that Fisetin can be administered in a pulsatile fashion before or after viral infection to reduce mortality of old organisms.

Discussion

Our study demonstrates that SnC are primed to respond to PAMPs by expressing and secreting even higher levels of inflammatory SASP factors. These PAMPs include the SARS-CoV-2 spike protein-1, which exacerbates the SASP of human SnC and, in turn, reduces innate viral defenses and increases expression of SARS-CoV-2 viral entry proteins in non-senescent human lung cells and tissue. Based on these observations, we formulated the "Amplifier/Rheostat" Hypothesis, whereby PAMPs, such as SARS-CoV-2 S1 viral antigen, cause a shift in the SASP of pre-existing SnC into a more highly inflammatory, pro-fibrotic SASP (Fig. 6). The amplified SASP factors include cytokines and chemokines, such as IL-1α, that exacerbate systemic inflammation and drive secondary senescence. These secondary SnC can then: 1) further exacerbate and prolong inflammation; 2) reduce viral defenses in non-SnC; 3) facilitate viral entry in non-SnC; 4) attenuate or delay recovery; 5) contribute to persistent frailty; 6) cause tissue fibrosis; and 7) contribute to hyperinflammation and multi-organ failure.

Our Amplifier/Rheostat hypothesis is supported by in vivo results, first by using acute LPS treatment and subsequently by exposing old mice to a normal microbial environment (NME), which includes a mouse β-coronavirus related to SARS-CoV-2. We demonstrate that the SnC burden in old mice confers, at least in part, the reduced resilience, increased inflammation, impaired immune response, and mortality observed in old male and female mice exposed to new viral pathogens. Both the pharmacological (e.g., senolytics Fisetin or D+Q) and genetic (*INK-ATTAC*) clearance of SnC

yielded significant delay, or in the case of the former reduction in mortality in both old male and female mice. Adverse outcomes were attenuated when the senolytic, Fisetin, was administered either prior to (a preventative measure) or after (a therapeutic intervention) NME exposure. The senolytics Fisetin and D+Q were more effective at delaying mortality than genetic ablation of SnC in the *INK-ATTAC* mice (Fig. 5F versus 5D), consistent with the fact that the latter only removes SnC expressing high levels of $p16^{Ink4a}$, not p16-low or -negative SnC. However, subtle differences in fomite bedding make it difficult to compare lifespan data between experiments.

Although the NME paradigm does not directly model SARS-CoV-2 infection, NME exposure involves transmission of multiple common community-acquired mouse infectious agents. Among these is the β-coronavirus MHV, which is an enteric virus transmitted by oral/fecal spread rather than respiratory droplets. Even though MHV infects hepatocytes to a greater extent than pulmonary tissue, we did find evidence of inflammation in the lung, spleen, liver, gastrointestinal tract, and kidney, similar to COVID-19 patients. MHV was a primary viral pathogen transferred by the NME as evidenced by serology, qRT-PCR, and liver histopathology, and caused severe disease in aged, but not young, mice. Furthermore, MHV immunization conferred protection from NME-induced mortality, indicating an essential role for the β-coronavirus in the mortality of old mice. The NME model does accurately reflect the dramatic response of naïve organisms to a novel β-coronavirus, the age disparity in outcomes observed in COVID-19 patients, the hyperinflammation elicited in some hosts, and the common experience of opportunistic infections contributing to disease severity and mortality.

SnC burden is increased in old and young mice exposed to NME (Fig. 3B) and, if it persists, could lead to additional co-morbidities. However, the magnitude of senescence in young animals appears not to reach a threshold that compromises survival. Thus, it is possible that senolytic treatment could be beneficial to COVID-19 survivors for improving long-term outcomes and suggests that monitoring expression of senescence markers in this patient population would be advantageous. Moreover, it is notable that it was not necessary to reduce senescence markers to the level of young individuals to dramatically improve survival. This supports the possibility that there is a threshold beyond which senescent cell burden is deleterious (*13*, *45*) and illustrates that, unlike for cancer cells, not every SnC needs to be eliminated to have a beneficial effect.

A high SnC burden in the elderly or those with chronic diseases such as diabetes, obesity, hypertension, or chronic lung disease likely can interfere with the ability of the immune system to induce a strong B and T cell response to novel antigens. We found that intermittent senolytic treatment

improved the development of an anti-MHV antibody response. This could be because the old mice survive long enough to mount a healthy response analogous to younger mice, or because dampening the SASP/inflammation improved immune cell function, or both. However, our preclinical data suggest that senolytics could improve the response of the elderly to vaccines for SARS-CoV-2 and others.

The immediate implication of these studies is that senolytics could have clinical application for attenuating mortality and other adverse outcomes in the elderly and those with comorbidities who become infected with SARS-CoV-2. Furthermore, based upon our findings in LPS-treated SnCs and aged mice, senolytics may be of potential therapeutic use for elderly persons stricken by bacterial infections. In addition, our data support the view that targeting pillars of aging and, in particular, cellular senescence, can improve resilience of the elderly in the face of viral pathogens. This strongly supports the Geroscience Hypothesis that targeting fundamental aging mechanisms can improve health span in the elderly and implies that targeting other pillars of aging might also alleviate morbidity due to viral infection. Thus, for the COVID-19 pandemic as well as future pandemics, rapalogs, glucocorticoids, and metformin, all of which inhibit the SASP, might lessen SARS-CoV-2 cytokine storm and improve outcomes (*46–48*). However, unlike senolytics, some of these drugs may need to be administered continuously or at least more frequently, adding to off-target and side effects, especially in elderly patients with co-morbidities and polypharmacy. Importantly, the SASP Amplifier Hypothesis, supported by data presented here, led to the initiation of a clinical trial (NCT04476953) to test whether Fisetin prevents disease progression in hospitalized older COVID-19 patients. A similar, but larger multi-site trial to test Fisetin in elderly COVID-19 patients in nursing homes (NCT04537299) also has been initiated. Finally, it is important to note that although there are now vaccines for SARS-CoV-2 being distributed, it will take a long time for a significant percentage of the world's population to be vaccinated. Even if the 95% effectiveness rate of the vaccines in healthy populations is borne out in elderly nursing home residents, still at least 1 out of 20 vaccinated elderly residents is anticipated to become infected by COVID-19 and will need treatment, potentially with senolytics and anti-virals.

Material and methods
Animals
Wild-type C57BL/6 (young = 2-7 months of age; old = 20 months of age or older) mice were bred at the University of Minnesota or Mayo Clinic, purchased from Charles River (Wilmington, MA), Jackson Laboratory (Bar Harbor, ME), or received from the Aging Rodent Colony at the National Institute of Aging (Baltimore, MD). C57BL/6:FVB mice and $Ercc1^{-/\Delta}$ mice were bred in the Niedernhofer laboratory at the University of Minnesota as previously described (*49*). The generation and characterization of the *INK-ATTAC* transgenic mouse line has been described (*42*). J.L.K., T.T., J.M. van Deursen, and D.J. Baker (all Mayo Clinic) designed the *INK-ATTAC* strategy. Pet store mice were purchased from local pet stores in the Minneapolis-St. Paul, MN metropolitan area. All mice were housed in AALAC-approved animal facilities at the University of Minnesota (BSL-1/-2 for SPF mice and BSL-3 for exposure to a natural microbial experience) or Mayo Clinic. Mice were randomly assigned to control or experimental groups based on weight and appearance. Experimental procedures were approved by the University of Minnesota and Mayo Clinic Institutional Animal Care and Use Committees and performed following the Office of Laboratory Animal Welfare guidelines and PHS Policy on Use of Laboratory Animals.

Mouse experiments
LPS challenge: WT mice were injected intraperitoneally with either LPS (500 ng/kg) or vehicle (PBS). Animals were euthanized 24 hours post-injection and tissues collected. Total RNA was isolated from kidney and liver for the analysis of senescence and SASP marker expression by quantitative PCR (qPCR) using the ΔΔCt method, with *Gapdh* serving as a housekeeping control. Serum levels of IL-6, MCP-1, TNFα were analyzed by ELISA.

Normal microbial experience (NME)
Immune-experienced mice were obtained from different vendors around Minneapolis, MN and were used as carriers of transmissible pathogens (hereafter called pet mice). Laboratory strains of mice were either directly cohoused with pet mice (*37*) or were housed on soiled bedding (totaling 150-300 cm^3/cage) that were collected from cages of pet store mice after 1 week of housing (fomites). Mice were housed in AALAC-approved ABSL3 animal facilities at the University of Minnesota and were monitored daily.

Senolytic preparation and administration
Fisetin (Indofine Chemical) or Dasatinib (LC laboratories. Cat# D-337, Woburn, MA) and Quercetin (Sigma. cat# Q4951-10G, St. Louis, MO) were dissolved in vehicle (10% ethanol, 30% polyethylene glycol 60% phosal 50 pg). Mice were weighed and given Fisetin (20 mg/kg), D+Q (5mg/kg+50mg/kg respectively), or vehicle control alone as indicated. Fisetin (500 ppm) was compounded into mouse chow (standard mouse diet, Lab Diet 5053). AP20187 was purchased from Clontech (Mountain View, CA). Vehicle (10% ethanol, 30% polyethylene glycol 60% phosal 50 pg) or AP20187 dissolved in vehicle was injected IP (10 mg/kg).

Tissue harvest

For RNA extraction, tissues were snap-frozen in liquid nitrogen and kept frozen until nucleic acid isolation. For histopathology, tissues were fixed in formalin and paraffin embedded.

Serology and measurement of viral RNA

Serum was collected at the indicated times for antibody screening using EZ-spot followed by a multiplexed fluorometric immunoassay (Charles River). The screening panel includes: mouse hepatitis virus (MHV), Sendai virus, pneumonia virus of mice, minute virus of mice (MVM), mouse parvovirus type 1(MPV), mouse parvovirus type 2, mouse parvovirus-NS1, murine norovirus (MNV), Theiler's murine encephalomyelitis virus (TMEV), reovirus, rotavirus EDIM, lymphocytic choriomeningitis virus, ectromelia virus, mouse adenovirus 1 and 2, mouse cytomegalovirus, polyoma virus, *Mycoplasma pulmonis*, *Enchephalitozoon cuniculi*, cilia-associated respiratory bacillus, and *Clostridium piliforme*. Relative serology scores for MHV antigens (recombinant A59-strain nucleocapsid protein, purified A-59 viral lysate, and purified S-strain viral lysate) were calculated by Charles River using median fluorescence index. Active pathogen infection was measured by PCR Rodent Infectious Agent (PRIA) array methods (Charles River) in samples collected from oral swabs or fecal material. This panel screened for MHV, MNV, MPV, MVM, *Rodentibacter heylii*, and *Helicobacter* species.

Infection with MHV-A59

MHV-A59 virus was a kind gift of Dr. Stan Perlman (U of Iowa). Virus was propagated and tittered onto 17cl-1 cells. Doses of $6 \times 10^5 - 1 \times 10^6$ PFU were delivered intra-nasally after briefly anesthetizing mice with Isoflurane.

Histology

Formalin-fixed samples were processed and embedded in paraffin before being sectioned (4 μm) and stained with hematoxylin and eosin. MHV immunohistochemistry was performed using anti-MHV-JHM ascitic fluid (*50*) (gift from Dr. S. Compton, Yale University) and bound antibody was detected using the Dako ARK Peroxidase kit (Animal Research Kit, Code K3954) for detecting mouse primary antibodies (Agilent Dako, Carpinteria, CA). All histologic sections were analyzed by two board-certified veterinary pathologists (TWC, MGO'S).

Serum cytokines and chemokines

Serum samples were analyzed by the Cytokine Reference Laboratory (CRL, University of Minnesota). Samples were analyzed for mouse specific IP10, IL-6, IL-1β, KC, IL-2, IFNγ, TNFα, LIX, MCP-1 MIP2, MIP1α, GMCSF, IL-10, and eotaxin using the multi-plex Luminex platform. Magnetic bead sets (cat. # MPTMAG-70K-14) were purchased from EMD Millipore (Burlington, MA). Proteins were measured according to the manufacturer's instructions. The beads were read on a Luminex instrument (Bioplex 200). Samples were run in duplicate and values were interpolated from 5-parameter-fitted standard curves. Serum concentrations of IL-6 (Abcam cat.# ab222503) and MCP-1 (Raybiotech cat.# ELM-MCP1-CL1, Peachtree Corners, GA) in LPS- and vehicle-treated mice (Fig. 1 and figs. S2 and S3) were measured by single-analyte ELISAs with a Varioskan plate reader. Samples were run in duplicate.

Measurement of cytokines and chemokines in liver

100 mg of tissue was homogenized in RIPA buffer and Complete Mini EDTA-free Protease Inhibitor and adjusted to 1 mg/mL. Samples were analyzed for mouse-specific IL-1β (Abcam cat.# ab197742, Cambridge, MA), IL-6 (Abcam cat.# ab222503), MCP-1 (Raybiotech cat.# ELM-MCP1-CL1), and TNFα (Abcam cat.# ab208348) by ELISA.

Cell culture

The kidney endothelial cells were from a female (21-week old) donor. Preadipocytes were isolated from abdominal subcutaneous fat biopsies obtained from 10 subjects (3 male; 7 female; median age 44.3 ± 9.2 years; BMI 44.6 ± 9.2) who underwent gastric bypass surgery. All subjects gave informed consent. The protocol was approved by the Mayo Clinic Institutional Review Board for Human Research. Cells were isolated, cultured, and made senescent as previously described (*12*). Human primary renal glomerular endothelial cells, ScienCell (Cat #4000, Carlsbad, CA), Human Small Airway Epithelial Cells (Cat# CC-2547, Lonza), and HUVECs (Lonza, Cat #CC-2519, Basel, Switzerland) were purchased and cultured following manufacturer's instructions. Cells were treated with S1 antigen (RayBiotech, Cat #230-30162-100, Peachtree Corners, GA), LPS from E.coli O111:B4 purified by ion-exchange chromatography (Millipore Sigma, Cat#L3024), or antibodies for INF-α, for different durations as described in the manuscript. Briefly, senescent and non-senescent cells were treated with LPS for 3 hours. Cells were washed, and RNA was collected. Endothelial cells were treated with viral antigen for 24 hours, cells were washed and medium was replaced with fresh MEM containing 2% FBS for collecting conditioned medium (CM) after 24 hours. CM was filtered and cytokine and chemokine protein levels in CM were measured using Luminex xMAP technology. The multiplexing analysis was performed using the Luminex 100 system (Luminex, Austin, TX) by Eve Technologies Corp. (Calgary, Alberta, Canada). Human multiplex kits were from Millipore (Billerica, MA).

Cell culture with conditioned media (CM) and recombinant IL-1α

Non-senescent human primary renal glomerular endothelial cells were co-cultured with CM from senescent or non-senescent human primary renal glomerular endothelial cells with or without neutralizing antibodies for IL-1α (Catalogue #7D4 Anti-hIL-1α-IgG, InvivoGen, San Diego, CA), IL-18 (Catalogue #PA5-47803, Thermo-Fisher, Waltham, MA), and PAI1 (Catalogue #MAB1786, R&D system, Minneapolis, MN) for 48 hours, and cells were collected for qPCR. Non-senescent human primary renal glomerular endothelial cells were co-cultured with recombinant human IL-1α protein (Catalogue #200-LA-010, R&D Systems, Minneapolis, MN) for 48 hours and cells were collected for qPCR.

Lung biopsies

Methods for acquisition of human lung samples have been described previously (*51*, *52*). Following pre-surgical patient consent, lung specimens were obtained from resections incidental to thoracic surgery at Mayo Clinic Rochester for clinical indications of focal, non-infectious causes (typically lobectomies, rarely pneumonectomies, for focal cancers). Normal lung areas were identified with a pathologist (protocol approved by the Mayo Clinic Institutional Review Board). Samples were formalin-fixed and paraffin-embedded for immunostaining and histology. Subjects used in this study were one female, four males, age 65.4 ± 10 years old (mean ± SD). The remaining clinical information was de-identified prior to immunostaining.

Immunostaining

Slides were rehydrated with xylene and decreasing concentrations of ethanol in water, blocked with endogenous peroxidase with 3% H_2O_2, and boiled for antigen retrieval in citrate buffer (pH 6.0). Sections were blocked with BSA 5% normal goat serum for 1 hour followed by overnight incubation with p16^{INK4a} mouse anti-human antibody (Roche Diagnostic, Clone E6H4, #705-4793, Rotkreuz, Switzerland). After washing in TBST buffer, sections were incubated in goat anti-mouse HRP antibody (Invitrogen, Cat #31430, Carlsbad, CA) for 30 min in blocking buffer and stained with TSA Cy5 (Akoya Biosciences, Cat #NEL745001KT, Menlo Park, CA) for 10 min. Antibodies were stripped with a second round of antigen retrieval in citrate buffer (pH 6.0) following the TSA manufacturer's protocol. After blocking steps, slides were incubated with rabbit anti-human TMPRSS2 antibody (#ab92323, Abcam) for 12 hours, washed, and incubated with secondary goat anti-rabbit HRP antibody (#31460, Invitrogen) for 30 min followed by 10 min of TSA FITC (Akoya Biosciences Cat #NEL741001KT). Slides were mounted in Prolong Gold anti-fade with DAPI (Thermo-Fisher Cat #P36935).

Imaging

Imaging was performed using a Nikon T1 microscope (Nikon, Japan). A total of 10 images of the alveolar region of lungs were captured/slide. Background correction and intensity thresholding were defined using controls and applied to all samples using Advanced NIS Elements software (Nikon, Tokyo, Japan), with fine-adjustments for each subject's background intensity. A total of 4-5 sections/slide with the best tissue integrity were selected for counting, and merged images were exported to ImageJ FIJI (*9*). We applied a centralized grid of 125 μm × 125 μm, generating 15 fields/section. TMPRSS2$^+$ and p16^{INK4a+} cell counting markers were used to retrieve cell numbers in each square. The single-channel for DAPI was exported to ImageJ and the same 125 μm × 125 μm grid was applied, so nuclei could be counted in each square slice.

RNA extraction

Tissues were snap-frozen after harvest. RNA was extracted using Trizol after homogenization in a bead beater. After homogenization, chloroform was added to each sample. Samples were centrifuged to separate the aqueous layer. RNA was purified using columns (PureLink RNA Mini Kit Cat#12183018A) according to the manufacturer's instructions. Concentration and purity of samples were assayed using a Nanodrop spectrophotometer.

RT-PCR and qPCR

Each cDNA sample was generated by reverse transcription using 1-2000 ng RNA and by following the recommended protocol from the manufacturer (High-capacity cDNA Reverse Transcription Kit; Thermo-Fisher Cat #4368813). A standard reverse transcription program was used (10 min at 25°C, 120 min at 37°C, 5 min at 85°C, held at 4°C). qPCR was performed using Taqman Fast Advanced Master Mix (Thermo-Fisher, Cat# numbers listed in supplemental table S3) and probes or PowerUp SYBR Green Master Mix and primer pairs. *Gapdh* was used as a control for gene expression analysis. Data were analyzed using the ΔΔCt method.

Statistical analysis

All data analyses were conducted in STATA 16.0 (College Station, TX: Stata Corp LLC). All figures were plotted using Prism 9.0 (GraphPad) or R 3.6.2. P value ≤ 0.05 was considered statistically significant.

To test the normality of the distribution of original variables (for analysis of variance [ANOVA] and Student's *t*-test) or residuals (for linear mixed model), skewness and kurtosis tests were performed accordingly (*53*). If the normality assumption was rejected (i.e., $P < 0.05$), we used zero-skewness log transformation (*54*). Then we performed the normality test again. If it was still rejected, we used a Box-Cox power

transformation. If neither of these worked, we used rank transformation (i.e., using the rank of the original variable) instead ([55]).

Student's *t*-test was used to compare the equality of means from two independent samples, while one-way ANOVA was used to compare means from multiple samples. Two-way ANOVA was used when there were two predictors and above. A linear mixed model was used if there was non-independence within individuals or experiments. Tukey HSD test was used for post-hoc multiple-comparison after one- or two-way ANOVA ([56], [57]). In the case of mixed-effect models, "margins" command was used to calculate statistics from predictions of the fitted model at fixed values of some predictors (e.g., treatment and type of cells). Partial Pearson correlation and linear regression, both with adjustment for strain ID, were performed to examine the association between $TMPRSS^{2+}$ and $p16^{INK4a+}$. To assess whether the SASP factors changed as a group, we created a composite score for each individual, which is the average z-score of the involved factors and performed the mixed effect model using the composite score as the outcome to assess whether the SASP factors changes as a group varied across covariates ([58])

$$\text{Composite Score}_i = \sum_{j=1}^{m_i} \frac{z_{ij}}{m_i}$$

where z_{ij} is the z-score of transformed values (by either log-transformed, Box-Cox transformed, or rank transformed) of SASP factor j for individual i, respectively. m_i is the number of observed factors for individual i.

For survival data, Kaplan-Meier survival curves were used to describe the survival process, which was followed by a log-rank test for assessing the equality of survivor functions between groups if there was only one predictor, or a Cox proportional hazards model if there were two predictors. Interaction between two predictors (e.g., treatment and type of cells) was considered in the above analyses if the original design was a factorial one.

REFERENCES AND NOTES

1. J. M. Jin, P. Bai, W. He, F. Wu, X.-F. Liu, D.-M. Han, S. Liu, J.-K. Yang, Gender Differences in Patients With COVID-19: Focus on Severity and Mortality. *Front. Public Health* **8**, 152 (2020). doi:10.3389/fpubh.2020.00152 Medline
2. C. Gebhard, V. Regitz-Zagrosek, H. K. Neuhauser, R. Morgan, S. L. Klein, Impact of sex and gender on COVID-19 outcomes in Europe. *Biol. Sex Differ.* **11**, 29 (2020). doi:10.1186/s13293-020-00304-9 Medline
3. L. Palaiodimos, D. G. Kokkinidis, W. Li, D. Karamanis, J. Ognibene, S. Arora, W. N. Southern, C. S. Mantzoros, Severe obesity, increasing age and male sex are independently associated with worse in-hospital outcomes, and higher in-hospital mortality, in a cohort of patients with COVID-19 in the Bronx, New York. *Metabolism* **108**, 154262 (2020). doi:10.1016/j.metabol.2020.154262 Medline
4. Q. Ruan, K. Yang, W. Wang, L. Jiang, J. Song, Clinical predictors of mortality due to COVID-19 based on an analysis of data of 150 patients from Wuhan, China. *Intensive Care Med.* **46**, 846–848 (2020). doi:10.1007/s00134-020-05991-x Medline
5. C. Huang, Y. Wang, X. Li, L. Ren, J. Zhao, Y. Hu, L. Zhang, G. Fan, J. Xu, X. Gu, Z. Cheng, T. Yu, J. Xia, Y. Wei, W. Wu, X. Xie, W. Yin, H. Li, M. Liu, Y. Xiao, H. Gao, L. Guo, J. Xie, G. Wang, R. Jiang, Z. Gao, Q. Jin, J. Wang, B. Cao, Clinical features of patients infected with 2019 novel coronavirus in Wuhan, China. *Lancet* **395**, 497–506 (2020). doi:10.1016/S0140-6736(20)30183-5 Medline
6. P. D. Robbins, D. Jurk, S. Khosla, J. L. Kirkland, N. K. LeBrasseur, J. D. Miller, J. F. Passos, R. J. Pignolo, T. Tchkonia, L. J. Niedernhofer, Senolytic Drugs: Reducing Senescent Cell Viability to Extend Health Span. *Annu. Rev. Pharmacol. Toxicol.* **61**, 779–803 (2021). doi:10.1146/annurev-pharmtox-050120-105018 Medline
7. V. Gorgoulis, P. D. Adams, A. Alimonti, D. C. Bennett, O. Bischof, C. Bishop, J. Campisi, M. Collado, K. Evangelou, G. Ferbeyre, J. Gil, E. Hara, V. Krizhanovsky, D. Jurk, A. B. Maier, M. Narita, L. Niedernhofer, J. F. Passos, P. D. Robbins, C. A. Schmitt, J. Sedivy, K. Vougas, T. von Zglinicki, D. Zhou, M. Serrano, M. Demaria, Cellular Senescence: Defining a Path Forward. *Cell* **179**, 813–827 (2019). doi:10.1016/j.cell.2019.10.005 Medline
8. J. L. Kirkland, T. Tchkonia, Cellular Senescence: A Translational Perspective. *EBioMedicine* **21**, 21–28 (2017). doi:10.1016/j.ebiom.2017.04.013 Medline
9. T. Tchkonia, Y. Zhu, J. van Deursen, J. Campisi, J. L. Kirkland, Cellular senescence and the senescent secretory phenotype: Therapeutic opportunities. *J. Clin. Invest.* **123**, 966–972 (2013). doi:10.1172/JCI64098 Medline
10. J. L. Kirkland, T. Tchkonia, Y. Zhu, L. J. Niedernhofer, P. D. Robbins, The Clinical Potential of Senolytic Drugs. *J. Am. Geriatr. Soc.* **65**, 2297–2301 (2017). doi:10.1111/jgs.14969 Medline
11. L. G. P. L. Prata, I. G. Ovsyannikova, T. Tchkonia, J. L. Kirkland, Senescent cell clearance by the immune system: Emerging therapeutic opportunities. *Semin. Immunol.* **40**, 101275 (2018). doi:10.1016/j.smim.2019.04.003 Medline
12. Y. Zhu, T. Tchkonia, T. Pirtskhalava, A. C. Gower, H. Ding, N. Giorgadze, A. K. Palmer, Y. Ikeno, G. B. Hubbard, M. Lenburg, S. P. O'Hara, N. F. LaRusso, J. D. Miller, C. M. Roos, G. C. Verzosa, N. K. LeBrasseur, J. D. Wren, J. N. Farr, S. Khosla, M. B. Stout, S. J. McGowan, H. Fuhrmann-Stroissnigg, A. U. Gurkar, J. Zhao, D. Colangelo, A. Dorronsoro, Y. Y. Ling, A. S. Barghouthy, D. C. Navarro, T. Sano, P. D. Robbins, L. J. Niedernhofer, J. L. Kirkland, The Achilles' heel of senescent cells: From transcriptome to senolytic drugs. *Aging Cell* **14**, 644–658 (2015). doi:10.1111/acel.12344 Medline
13. M. Xu, T. Pirtskhalava, J. N. Farr, B. M. Weigand, A. K. Palmer, M. M. Weivoda, C. L. Inman, M. B. Ogrodnik, C. M. Hachfeld, D. G. Fraser, J. L. Onken, K. O. Johnson, G. C. Verzosa, L. G. P. Langhi, M. Weigl, N. Giorgadze, N. K. LeBrasseur, J. D. Miller, D. Jurk, R. J. Singh, D. B. Allison, K. Ejima, G. B. Hubbard, Y. Ikeno, H. Cubro, V. D. Garovic, X. Hou, S. J. Weroha, P. D. Robbins, L. J. Niedernhofer, S. Khosla, T. Tchkonia, J. L. Kirkland, Senolytics improve physical function and increase lifespan in old age. *Nat. Med.* **24**, 1246–1256 (2018). doi:10.1038/s41591-018-0092-9 Medline
14. M. J. Yousefzadeh, Y. Zhu, S. J. McGowan, L. Angelini, H. Fuhrmann-Stroissnigg, M. Xu, Y. Y. Ling, K. I. Melos, T. Pirtskhalava, C. L. Inman, C. McGuckian, E. A. Wade, J. I. Kato, D. Grassi, M. Wentworth, C. E. Burd, E. A. Arriaga, W. L. Ladiges, T. Tchkonia, J. L. Kirkland, P. D. Robbins, L. J. Niedernhofer, Fisetin is a senotherapeutic that extends health and lifespan. *EBioMedicine* **36**, 18–28 (2018). doi:10.1016/j.ebiom.2018.09.015 Medline
15. P. Mehta, D. F. McAuley, M. Brown, E. Sanchez, R. S. Tattersall, J. J. Manson; HLH Across Speciality Collaboration, UK, COVID-19: Consider cytokine storm syndromes and immunosuppression. *Lancet* **395**, 1033–1034 (2020). doi:10.1016/S0140-6736(20)30628-0 Medline
16. A. G. Laing, A. Lorenc, I. Del Molino Del Barrio, A. Das, M. Fish, L. Monin, M. Muñoz-Ruiz, D. R. McKenzie, T. S. Hayday, I. Francos-Quijorna, S. Kamdar, M. Joseph, D. Davies, R. Davis, A. Jennings, I. Zlatareva, P. Vantourout, Y. Wu, V. Sofra, F. Cano, M. Greco, E. Theodoridis, J. D. Freedman, S. Gee, J. N. E. Chan, S. Ryan, E. Bugallo-Blanco, P. Peterson, K. Kisand, L. Haljasmägi, L. Chadli, P. Moingeon, L. Martinez, B. Merrick, K. Bisnauthsing, K. Brooks, M. A. A. Ibrahim, J. Mason, F. Lopez Gomez, K. Babalola, S. Abdul-Jawad, J. Cason, C. Mant, J. Seow, C. Graham, K. J. Doores, F. Di Rosa, J. Edgeworth, M. Shankar-Hari, A. C. Hayday, A dynamic COVID-19 immune signature includes associations with poor prognosis. *Nat. Med.* **26**, 1951 (2020). doi:10.1038/s41591-020-1038-6 Medline
17. M. J. Yousefzadeh, J. Zhao, C. Bukata, E. A. Wade, S. J. McGowan, L. A. Angelini, M. P. Bank, A. U. Gurkar, C. A. McGuckian, M. F. Calubag, J. I. Kato, C. E. Burd, P. D. Robbins, L. J. Niedernhofer, Tissue specificity of senescent cell accumulation during physiologic and accelerated aging of mice. *Aging Cell* **19**, e13094 (2020). doi:10.1111/acel.13094 Medline

18. J. Shang, Y. Wan, C. Luo, G. Ye, Q. Geng, A. Auerbach, F. Li, Cell entry mechanisms of SARS-CoV-2. *Proc. Natl. Acad. Sci. U.S.A.* **117**, 11727–11734 (2020). doi:10.1073/pnas.2003138117 Medline

19. M. Hoffmann, H. Kleine-Weber, S. Pöhlmann, A Multibasic Cleavage Site in the Spike Protein of SARS-CoV-2 Is Essential for Infection of Human Lung Cells. *Mol. Cell* **78**, 779–784.e5 (2020). doi:10.1016/j.molcel.2020.04.022 Medline

20. S. F. Dosch, S. D. Mahajan, A. R. Collins, SARS coronavirus spike protein-induced innate immune response occurs via activation of the NF-kappaB pathway in human monocyte macrophages in vitro. *Virus Res.* **142**, 19–27 (2009). doi:10.1016/j.virusres.2009.01.005 Medline

21. A. Huertas, D. Montani, L. Savale, J. Pichon, L. Tu, F. Parent, C. Guignabert, M. Humbert, Endothelial cell dysfunction: A major player in SARS-CoV-2 infection (COVID-19)? *Eur. Respir. J.* **56**, 2001634 (2020). doi:10.1183/13993003.01634-2020 Medline

22. K. Shirato, T. Kizaki, SARS-CoV-2 spike protein S1 subunit induces pro-inflammatory responses via toll-like receptor 4 signaling in murine and human macrophages. *Heliyon* **7**, e06187 (2021). doi:10.1016/j.heliyon.2021.e06187 Medline

23. M. Zheng, R. Karki, E. P. Williams, D. Yang, E. Fitzpatrick, P. Vogel, C. B. Jonsson, T.-D. Kanneganti, TLR2 senses the SARS-CoV-2 envelope protein to produce inflammatory cytokines. *Nat. Immunol.* (2021). doi:10.1038/s41590-021-00937-x Medline

24. A. Hernandez-Segura, T. V. de Jong, S. Melov, V. Guryev, J. Campisi, M. Demaria, Unmasking Transcriptional Heterogeneity in Senescent Cells. *Curr. Biol.* **27**, 2652–2660.e4 (2017). doi:10.1016/j.cub.2017.07.033 Medline

25. D. Blanco-Melo, B. E. Nilsson-Payant, W.-C. Liu, S. Uhl, D. Hoagland, R. Møller, T. X. Jordan, K. Oishi, M. Panis, D. Sachs, T. T. Wang, R. E. Schwartz, J. K. Lim, R. A. Albrecht, B. R. tenOever, Imbalanced Host Response to SARS-CoV-2 Drives Development of COVID-19. *Cell* **181**, 1036–1045.e9 (2020). doi:10.1016/j.cell.2020.04.026 Medline

26. L. A. Maciel-Barón, S. L. Morales-Rosales, A. A. Aquino-Cruz, F. Triana-Martínez, S. Galván-Arzate, A. Luna-López, V. Y. González-Puertos, N. E. López-Díazguerrero, C. Torres, M. Königsberg, Senescence associated secretory phenotype profile from primary lung mice fibroblasts depends on the senescence induction stimuli. *Age* **38**, 26 (2016). doi:10.1007/s11357-016-9886-1 Medline

27. M. Mariotti, S. Castiglioni, D. Bernardini, J. A. Maier, Interleukin 1 alpha is a marker of endothelial cellular senescent. *Immun. Ageing* **3**, 4 (2006). doi:10.1186/1742-4933-3-4 Medline

28. M. J. Schafer, T. A. White, K. Iijima, A. J. Haak, G. Ligresti, E. J. Atkinson, A. L. Oberg, J. Birch, H. Salmonowicz, Y. Zhu, D. L. Mazula, R. W. Brooks, H. Fuhrmann-Stroissnigg, T. Pirtskhalava, Y. S. Prakash, T. Tchkonia, P. D. Robbins, M. C. Aubry, J. F. Passos, J. L. Kirkland, D. J. Tschumperlin, H. Kita, N. K. LeBrasseur, Cellular senescence mediates fibrotic pulmonary disease. *Nat. Commun.* **8**, 14532 (2017). doi:10.1038/ncomms14532 Medline

29. D. M. Del Valle, S. Kim-Schulze, H.-H. Huang, N. D. Beckmann, S. Nirenberg, B. Wang, Y. Lavin, T. H. Swartz, D. Madduri, A. Stock, T. U. Marron, H. Xie, M. Patel, K. Tuballes, O. Van Oekelen, A. Rahman, P. Kovatch, J. A. Aberg, E. Schadt, S. Jagannath, M. Mazumdar, A. W. Charney, A. Firpo-Betancourt, D. R. Mendu, J. Jhang, D. Reich, K. Sigel, C. Cordon-Cardo, M. Feldmann, S. Parekh, M. Merad, S. Gnjatic, An inflammatory cytokine signature predicts COVID-19 severity and survival. *Nat. Med.* **26**, 1636–1643 (2020). doi:10.1038/s41591-020-1051-9 Medline

30. V. Bordoni, A. Sacchi, E. Cimini, S. Notari, G. Grassi, E. Tartaglia, R. Casetti, M. L. Giancola, N. Bevilacqua, M. Maeurer, A. Zumla, F. Locatelli, F. De Benedetti, F. Palmieri, L. Marchioni, M. R. Capobianchi, G. D'Offizi, N. Petrosillo, A. Antinori, E. Nicastri, G. Ippolito, C. Agrati, An Inflammatory Profile Correlates With Decreased Frequency of Cytotoxic Cells in Coronavirus Disease 2019. *Clin. Infect. Dis.* **71**, 2272–2275 (2020). doi:10.1093/cid/ciaa577 Medline

31. J. W. Song, C. Zhang, X. Fan, F.-P. Meng, Z. Xu, P. Xia, W.-J. Cao, T. Yang, X.-P. Dai, S.-Y. Wang, R.-N. Xu, T.-J. Jiang, W.-G. Li, D.-W. Zhang, P. Zhao, M. Shi, C. Agrati, G. Ippolito, M. Maeurer, A. Zumla, J.-Y. Zhang, Immunological and inflammatory profiles in mild and severe cases of COVID-19. *Nat. Commun.* **11**, 3410 (2020). doi:10.1038/s41467-020-17240-2 Medline

32. C. Jiang, G. Liu, T. Luckhardt, V. Antony, Y. Zhou, A. B. Carter, V. J. Thannickal, R.-M. Liu, Serpine 1 induces alveolar type II cell senescence through activating p53-

p21-Rb pathway in fibrotic lung disease. *Aging Cell* **16**, 1114–1124 (2017). doi:10.1111/acel.12643 Medline

33. Y. Zuo, M. Warnock, A. Harbaugh, S. Yalavarthi, K. Gockman, M. Zuo, J. A. Madison, J. S. Knight, Y. Kanthi, D. A. Lawrence, Plasma tissue plasminogen activator and plasminogen activator inhibitor-1 in hospitalized COVID-19 patients. *Sci. Rep.* **11**, 1580 (2021). doi:10.1038/s41598-020-80010-z Medline

34. A. V. Orjalo, D. Bhaumik, B. K. Gengler, G. K. Scott, J. Campisi, Cell surface-bound IL-1alpha is an upstream regulator of the senescence-associated IL-6/IL-8 cytokine network. *Proc. Natl. Acad. Sci. U.S.A.* **106**, 17031–17036 (2009). doi:10.1073/pnas.0905299106 Medline

35. C. Lucas, P. Wong, J. Klein, T. B. R. Castro, J. Silva, M. Sundaram, M. K. Ellingson, T. Mao, J. E. Oh, B. Israelow, T. Takahashi, M. Tokuyama, P. Lu, A. Venkataraman, A. Park, S. Mohanty, H. Wang, A. L. Wyllie, C. B. F. Vogels, R. Earnest, S. Lapidus, I. M. Ott, A. J. Moore, M. C. Muenker, J. B. Fournier, M. Campbell, C. D. Odio, A. Casanovas-Massana, R. Herbst, A. C. Shaw, R. Medzhitov, W. L. Schulz, N. D. Grubaugh, C. Dela Cruz, S. Farhadian, A. I. Ko, S. B. Omer, A. Iwasaki; Yale IMPACT Team, Longitudinal analyses reveal immunological misfiring in severe COVID-19. *Nature* **584**, 463–469 (2020). doi:10.1038/s41586-020-2588-y Medline

36. M. A. Huggins, F. V. Sjaastad, M. Pierson, T. A. Kucaba, W. Swanson, C. Staley, A. R. Weingarden, I. J. Jensen, D. B. Danahy, V. P. Badovinac, S. C. Jameson, V. Vezys, D. Masopust, A. Khoruts, T. S. Griffith, S. E. Hamilton, Microbial Exposure Enhances Immunity to Pathogens Recognized by TLR2 but Increases Susceptibility to Cytokine Storm through TLR4 Sensitization. *Cell Rep.* **28**, 1729–1743.e5 (2019). doi:10.1016/j.celrep.2019.07.028 Medline

37. M. A. Huggins, S. C. Jameson, S. E. Hamilton, Embracing microbial exposure in mouse research. *J. Leukoc. Biol.* **105**, 73–79 (2019). doi:10.1002/JLB.4RI0718-273R Medline

38. L. K. Beura, S. E. Hamilton, K. Bi, J. M. Schenkel, O. A. Odumade, K. A. Casey, E. A. Thompson, K. A. Fraser, P. C. Rosato, A. Filali-Mouhim, R. P. Sekaly, M. K. Jenkins, V. Vezys, W. N. Haining, S. C. Jameson, D. Masopust, Normalizing the environment recapitulates adult human immune traits in laboratory mice. *Nature* **532**, 512–516 (2016). doi:10.1038/nature17655 Medline

39. N. Khan, D. N. Syed, N. Ahmad, H. Mukhtar, Fisetin: A dietary antioxidant for health promotion. *Antioxid. Redox Signal.* **19**, 151–162 (2013). doi:10.1089/ars.2012.4901 Medline

40. V. M. Adhami, D. N. Syed, N. Khan, H. Mukhtar, Dietary flavonoid fisetin: A novel dual inhibitor of PI3K/Akt and mTOR for prostate cancer management. *Biochem. Pharmacol.* **84**, 1277–1281 (2012). doi:10.1016/j.bcp.2012.07.012 Medline

41. Y. Zhu, E. J. Doornebal, T. Pirtskhalava, N. Giorgadze, M. Wentworth, H. Fuhrmann-Stroissnigg, L. J. Niedernhofer, P. D. Robbins, T. Tchkonia, J. L. Kirkland, New agents that target senescent cells: The flavone, fisetin, and the BCL-X_L inhibitors, A1331852 and A1155463. *Aging* **9**, 955–963 (2017). doi:10.18632/aging.101202 Medline

42. D. J. Baker, T. Wijshake, T. Tchkonia, N. K. LeBrasseur, B. G. Childs, B. van de Sluis, J. L. Kirkland, J. M. van Deursen, Clearance of p16Ink4a-positive senescent cells delays ageing-associated disorders. *Nature* **479**, 232–236 (2011). doi:10.1038/nature10600 Medline

43. I. Murano, J. M. Rutkowski, Q. A. Wang, Y.-R. Cho, P. E. Scherer, S. Cinti, Time course of histomorphological changes in adipose tissue upon acute lipoatrophy. *Nutr. Metab. Cardiovasc. Dis.* **23**, 723–731 (2013). doi:10.1016/j.numecd.2012.03.005 Medline

44. H. Ragelle, S. Crauste-Manciet, J. Seguin, D. Brossard, D. Scherman, P. Arnaud, G. G. Chabot, Nanoemulsion formulation of fisetin improves bioavailability and antitumour activity in mice. *Int. J. Pharm.* **427**, 452–459 (2012). doi:10.1016/j.ijpharm.2012.02.025 Medline

45. J. L. Kirkland, T. Tchkonia, Senolytic drugs: From discovery to translation. *J. Intern. Med.* **288**, 518–536 (2020). doi:10.1111/joim.13141 Medline

46. B. Christy, M. Demaria, J. Campisi, J. Huang, D. Jones, S. G. Dodds, C. Williams, G. Hubbard, C. B. Livi, X. Gao, S. Weintraub, T. Curiel, Z. D. Sharp, P. Hasty, p53 and rapamycin are additive. *Oncotarget* **6**, 15802–15813 (2015). doi:10.18632/oncotarget.4602 Medline

47. R. M. Laberge, L. Zhou, M. R. Sarantos, F. Rodier, A. Freund, P. L. J. de Keizer, S. Liu, M. Demaria, Y.-S. Cong, P. Kapahi, P.-Y. Desprez, R. E. Hughes, J. Campisi, Glucocorticoids suppress selected components of the senescence-associated

secretory phenotype. *Aging Cell* **11**, 569–578 (2012). [doi:10.1111/j.1474-9726.2012.00818.x](#) [Medline](#)

48. N. Noren Hooten, A. Martin-Montalvo, D. F. Dluzen, Y. Zhang, M. Bernier, A. B. Zonderman, K. G. Becker, M. Gorospe, R. de Cabo, M. K. Evans, Metformin-mediated increase in DICER1 regulates microRNA expression and cellular senescence. *Aging Cell* **15**, 572–581 (2016). [doi:10.1111/acel.12469](#) [Medline](#)

49. A. Ahmad, A. R. Robinson, A. Duensing, E. van Drunen, H. B. Beverloo, D. B. Weisberg, P. Hasty, J. H. J. Hoeijmakers, L. J. Niedernhofer, ERCC1-XPF endonuclease facilitates DNA double-strand break repair. *Mol. Cell. Biol.* **28**, 5082–5092 (2008). [doi:10.1128/MCB.00293-08](#) [Medline](#)

50. S. W. Barthold, A. L. Smith, M. L. Povar, Enterotropic mouse hepatitis virus infection in nude mice. *Lab. Anim. Sci.* **35**, 613–618 (1985). [Medline](#)

51. A. J. Abcejo, V. Sathish, D. F. Smelter, B. Aravamudan, M. A. Thompson, W. R. Hartman, C. M. Pabelick, Y. S. Prakash, Brain-derived neurotrophic factor enhances calcium regulatory mechanisms in human airway smooth muscle. *PLOS ONE* **7**, e44343 (2012). [doi:10.1371/journal.pone.0044343](#) [Medline](#)

52. Y. S. Prakash, M. A. Thompson, B. Vaa, I. Matabdin, T. E. Peterson, T. He, C. M. Pabelick, Caveolins and intracellular calcium regulation in human airway smooth muscle. *Am. J. Physiol. Lung Cell. Mol. Physiol.* **293**, L1118–L1126 (2007). [doi:10.1152/ajplung.00136.2007](#) [Medline](#)

53. R. B. Dagostino, A. Belanger, R. B. Dagostino, A Suggestion for Using Powerful and Informative Tests of Normality. *Am. Stat.* **44**, 316–321 (1990). [doi:10.2307/2684359](#)

54. G. E. P. Box, D. R. Cox, An Analysis of Transformations. *J. R. Stat. Soc. B* **26**, 211–243 (1964). [doi:10.1111/j.2517-6161.1964.tb00553.x](#)

55. M. R. Harwell, R. C. Serlin, A nonparametric test statistic for general linear model. *J. Educ. Stat.* **14**, 351–371 (1989). [doi:10.3102/10769986014004351](#)

56. R. G. Miller, *Simultaneous statistical inference*. Springer series in statistics (Springer-Verlag, New York, ed. 2d, 1981), pp. xvi, 299 p.

57. J. W. Tukey, Comparing individual means in the analysis of variance. *Biometrics* **5**, 99–114 (1949). [doi:10.2307/3001913](#) [Medline](#)

58. H. J. Einhorn, R. M. Hogarth, Unit weighting schemes for decision making. *Organ. Behav. Hum. Perform.* **13**, 171–192 (1975). [doi:10.1016/0030-5073(75)90044-6](#)

ACKNOWLEDGMENTS

A

p16^{INK4a} | *p21^{CIP1}* | *IL1α* | *IL1β* | *IL6*

IL10 | *MCP1* | *PAI1* | *PAI2*

Legend: ● Non-SnC ● SnC

B

p16^{Ink4a} | *p21^{Cip1}* | *Il1α* | *Il1β* | *Il6*

Il10 | *Mcp1* | *Tnfα* | *Pai1* | *Pai2*
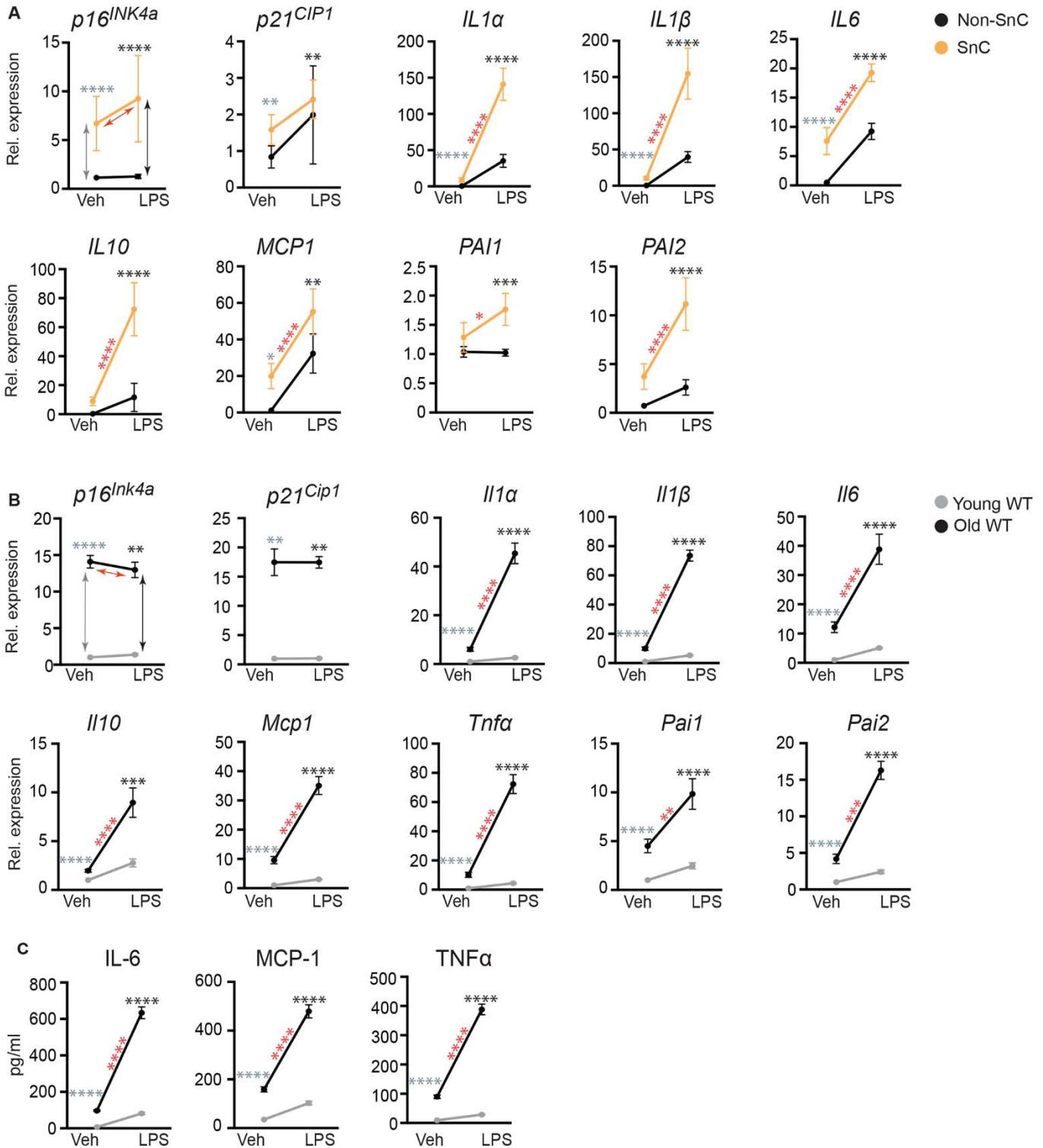
Legend: ● Young WT ● Old WT

C

IL-6 | MCP-1 | TNFα

Fig. 1. (previous page) The Senescence-Associated Secretory Phenotype (SASP) is amplified by Pathogen-Activated Molecular Pattern (PAMP) factors. (A) Human adipocyte progenitors isolated from subcutaneous fat biopsies were induced to undergo senescence with 10 Gy of ionizing radiation (SnC) or not (non-SnC) (n = 5 subjects). Cells were treated with 10 ng of the prototype PAMP, lipopolysaccharide (LPS) for 3 hours before RNA isolation. Gene expression was measured by qPCR and the expression in LPS-treated cells normalized to vehicle-treated samples. Means ± SEM. Statistical significance was calculated using a mixed effect model for the effect of LPS on SnC and its differential effects on SnC compared to non-SnC. Supplemental table S1 has details. Arrows and asterisks: gray = vehicle-treated SnC vs. non-SnC; black = LPS-treated SnC vs. non-SnC; red = SnC ± LPS. *$p < 0.05$, **$p < 0.01$, ***$p < 0.001$, ****$p < 0.0001$. (B) Young (2-month-old) and old (26-month-old) mice were treated with PBS (n = 5y and 5o) or LPS (n = 4y and 3o) and tissues collected 24 hours later. RNA was isolated from liver and gene expression measured by qPCR. Expression in LPS-treated mice was normalized to vehicle-treated animals. Means ± SEM, two-way ANOVA and *post-hoc* comparison Tukey's Honestly Significant Difference used to compare the two animal cohorts within a treatment group. Arrows and asterisks: gray = vehicle-treated old vs. young; black = LPS-treated old vs. young; red = old ± LPS. **$p < 0.01$, ***$p < 0.001$, ****$p < 0.0001$. Kidney data in fig. S2. (C) Serum protein from the same mice measured by ELISA. Statistics as described in B.

Fig. 2 (next page). The SARS-CoV2 spike protein-1 (S1) exacerbates the secretory phenotype of senescent human endothelial cells, decreasing viral defenses and elevating viral entry/processing gene expression. (A) Primary human kidney endothelial cells (n=9 biological replicates) were induced to undergo senescence with 10 Gy of ionizing radiation (SnC) or not (non-SnC) then treated with 500 ng recombinant S1 or PBS vehicle for 24 hours. Thirty SASP-related proteins were measured in the conditioned media (CM) by Luminex xMAP technology. Relative abundance induced by S1, normalized to vehicle treated non-senescent cells (non-SnC + Veh), is illustrated in the heat map. A mixed effects model was used to test the effect of S1, senescence, and their interaction, taking into account duplicate measures within a subject for each protein as well as the composite score. Margin effects of SnC in the treatment group also were tested under the mixed effects model framework. Overall, the effect of S1 on SnC was significantly more pronounced than on non-SnC (composite score change $p < 0.0089$; mean values and p values for each cytokine are in supplementary table S2). (B) Schematic of experiments in C, E, and F. Primary human cells were induced to undergo senescence with 10 Gy of ionizing radiation (SnC) or not (non-SnC). Twenty days later, CM was collected (n = 4 biological replicates) and used to treat non-SnC (n = 4 biological replicates) either with or without antibodies to IL-1α, IL-18, and PAI-1 (alone or in combination) for 48 hours, then RNA isolated to measure expression of genes related to SARS-CoV-2 pathogenesis by qPCR. Expression in cells treated with SnC CM was normalized to cells treated with non-SnC CM. Data displayed as mean ± SEM, mixed effects model. *$p < 0.05$ **$p < 0.01$, ***$p < 0.001$, ****$p < 0.0001$. (C). *IFITM* expression in human kidney endothelial cells treated with CM from SnC versus non-SnC human kidney endothelial cells. (D) *IFITM* expression in human kidney endothelial cells exposed to two concentrations of IL-1α (n = 4 biological replicates). Expression was normalized to vehicle-treated samples. (E) Gene expression in human lung epithelial cells treated with CM from SnC vs. non-SnC pre-adipocytes, HUVECs, or kidney endothelial cells. (F) *TMPRSS2* expression in human kidney endothelial cells treated with CM from SnC vs. non-SnC kidney endothelial cells with or without neutralizing antibodies or human kidney endothelial cells with recombinant IL-1α for 48 hours. (G) Human lung biopsies acquired for clinical indications of focal, non-infectious causes from elderly patients were stained for TMPRSS2, p16[INK4a], and DAPI to detect nuclei (n = 5 subjects). Representative images are shown. Scale bar = 20 μm. (H) TMPRSS2^{+}, p16[INK4a+], and total nuclei were counted and expressed as a function of total nuclei in each field. TMPRSS2^{+} and p16[INK4a+] cells/field were tightly linked ($p < 0.0001$; Partial Pearson correlation). Each color series of dots represents replicates from a single subject.
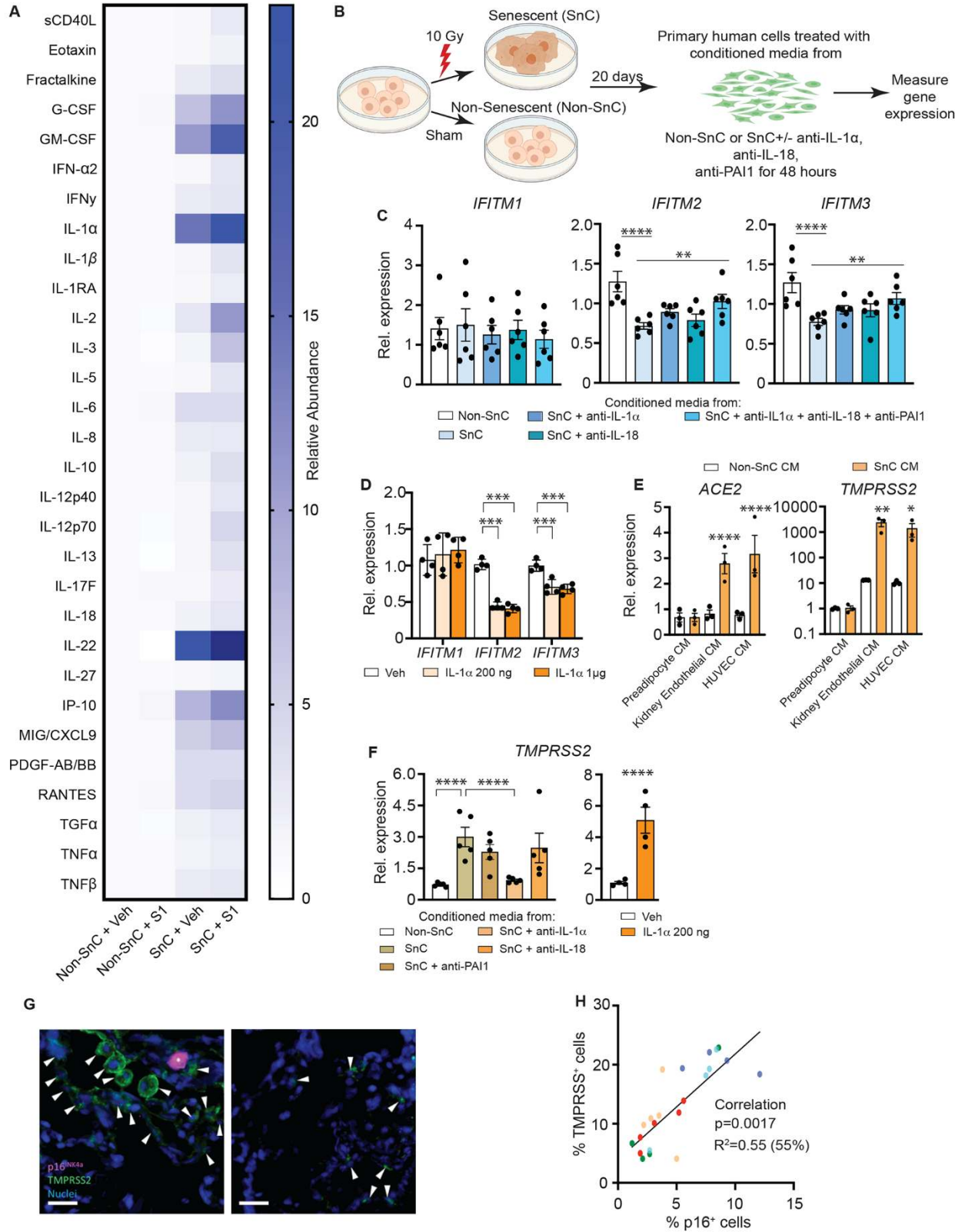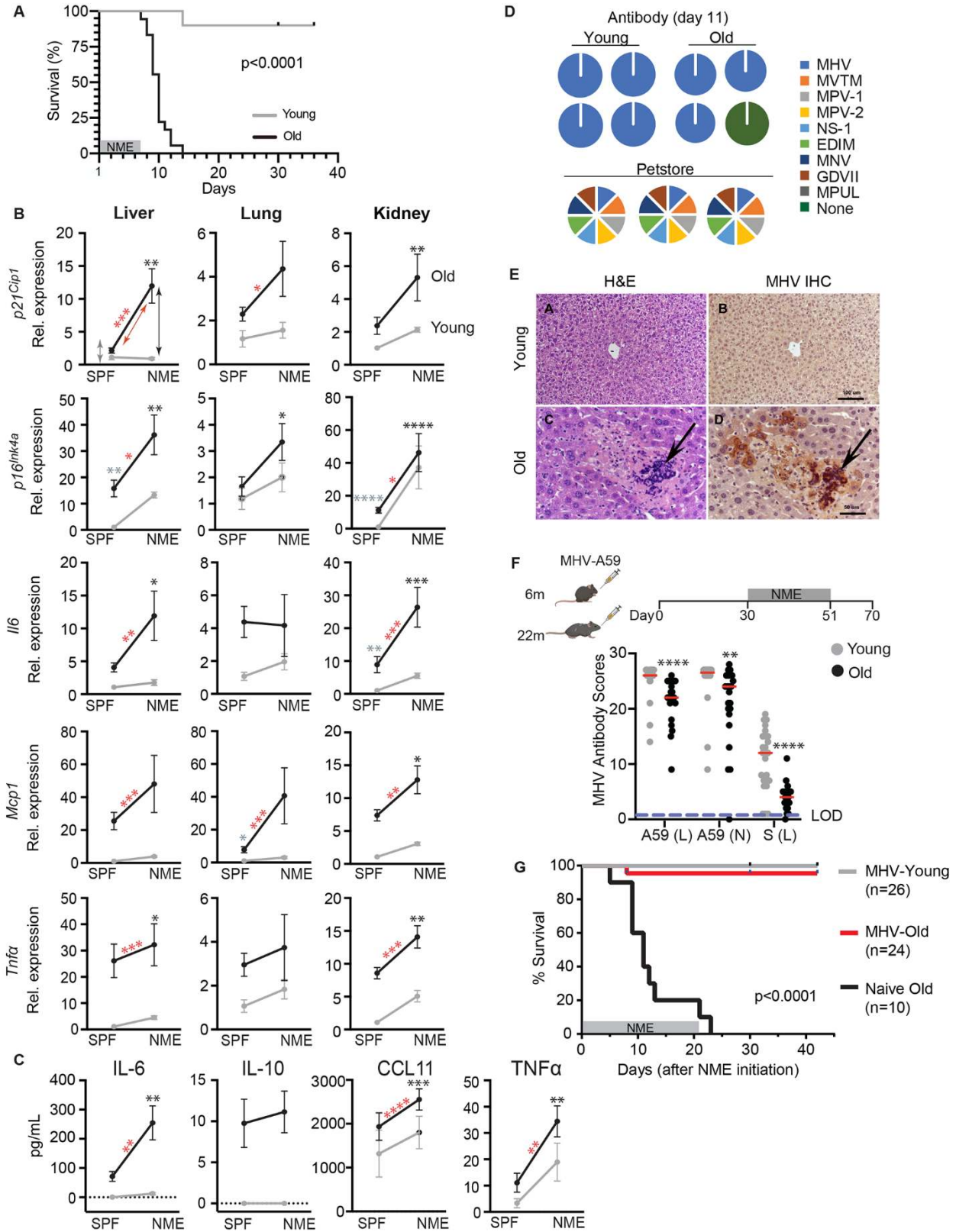
Fig. 3 (previous page). Old mice are vulnerable to a normal microbial experience (NME) that includes acute mouse β-coronavirus infection. (A) Young (3-month-old) and old (20-24-month-old) WT mice were exposed to NME bedding produced from pet store mice for 7 days. Survival was monitored for 35 days post-initiation of NME (n = 10 young; n = 18 old). Log-rank (Mantel Cox) test. (B) Gene expression in three tissues of SPF or NME (6-7-day exposure) young and old mice (n = 3 young SPF; n = 5 old SPF; n = 14 young NME; n = 13 old NME) measured by qPCR. Expression was normalized to young SPF mice. Means ± SEM, two-way ANOVA and *post-hoc* comparison Tukey's Honestly Significant Difference used to compare the two animal cohorts within a treatment group. *p < 0.05, **p < 0.01, ***p < 0.001, ****p < 0.0001. Arrows and asterisks: gray = SPF old versus young; black = NME old versus young; red = old SPF versus old NME. (C) Serum cytokine levels in young and old mice (n = 3 young SPF; n = 5 old SPF; n = 19 young NME; n = 17 old NME) measured by ELISA at day 5 post-NME. Statistics as described in B. (D) Serology to detect antibodies against microbes in NME bedding. To the right are the murine pathogens commonly tested for by Charles River Laboratory to define SPF housing. The pie charts illustrate the exposures detected in individual young and old mice (n = 24 young; n = 21-23 old) day 11 post-initiation of NME. Serology of pet store mice is illustrated below. (E) Representative images of H&E staining or MHV immunohistochemistry in liver sections from young and old mice exposed to NME. (F) (Top) Schematic to illustrate the experimental design. Young (6-month-old) or old (22-month-old) female mice were inoculated with a sublethal dose of MHV. Thirty days later, naïve and inoculated mice were exposed to NME bedding for 3 weeks. (Bottom) Serum antibodies against 3 different MHV antigens measured 21 days after MHV inoculation and reported as relative scores. The dotted line represents the limit of detection (LOD). Means ± SEM, unpaired two-tailed Student's *t* test. **p < 0.01, ****p < 0.0001. (G) Survival of MHV-inoculated and naïve mice measured for 42 days post-initiation of NME. Log-rank [Mantel Cox] test.

Fig. 4 (next page). Treatment with the senolytic Fisetin decreases mortality in NME-exposed old mice. (A) Schematic of the experiment. Young (6-7 months) and old (20-24 months) mice were exposed to NME bedding containing murine β-coronavirus MHV for 7 days. Mice were treated with 20 mg/kg/day Fisetin or vehicle only by oral gavage daily for 3 consecutive days starting on day 3 post-initiation of NME. The 3 days of treatment were repeated (3 days on, 4 days off) for 3 weeks. Animals were also fed standard chow with Fisetin added (500 ppm) *ad libitum* after initiation of treatment. (B) Survival was measured for 36 days following initiation of NME (n = 9 young + vehicle; n = 5 young + Fisetin; n = 18 old + vehicle; n = 19 old + Fisetin). Log-rank [Mantel Cox] test. p < 0.0001 for old mice ± Fisetin. (C) Relative MHV antibody score in young and old mice in B on the indicated day post-initiation of NME. (D to G) Young (2-month-old) and old (20-month-old) mice were exposed to NME bedding ± treatment with Fisetin as described in A. On day 8-9 post-initiation of NME, animals were euthanized, and tissues collected for measuring gene expression (n = 10 young + vehicle; n = 8-10 young + Fisetin; n = 10-11 old + vehicle; n = 13 old + Fisetin). All expression data were normalized to young mice treated with vehicle. Data displayed as means ± SEM, two-way ANOVA and *post-hoc* comparison Tukey's Honestly Significant Difference used to compare the two animal cohorts within a treatment group. Arrows and asterisks: gray = vehicle-treated old versus young; black = Fisetin-treated old versus young; red = old ± Fisetin. *p < 0.05, **p < 0.01, ***p < 0.001, ****p < 0.0001. (D) MHV mRNA was quantified by qPCR in fecal pellets collected from individual animals in C. (E) Quantification of *p16^{Ink4a}* and *p21^{Cip1}* mRNA in four tissues. (F) Quantification of SASP factor mRNA in liver. Data on other genes and tissues in fig. S9. (G) SASP protein levels in the liver measured by ELISA.
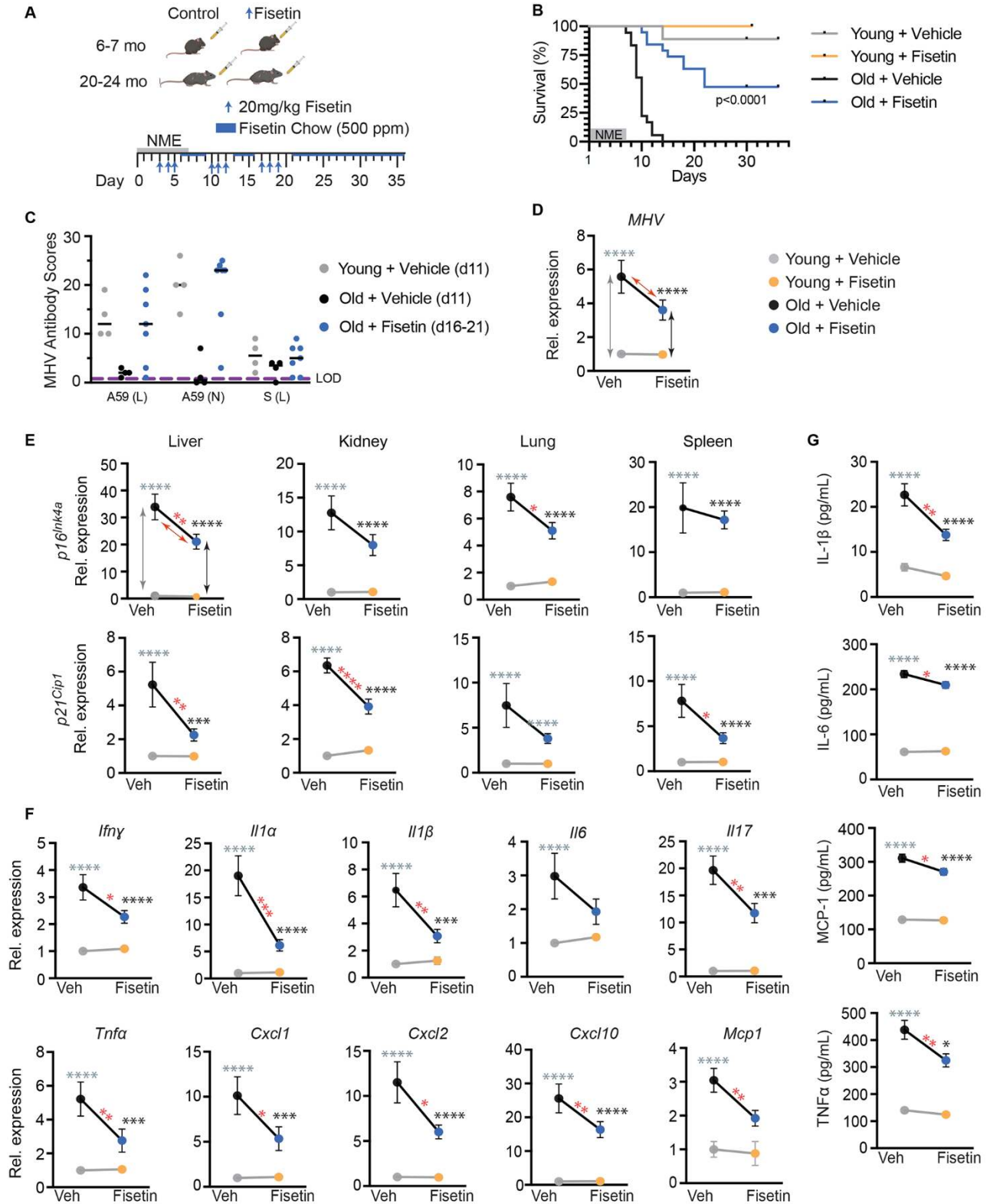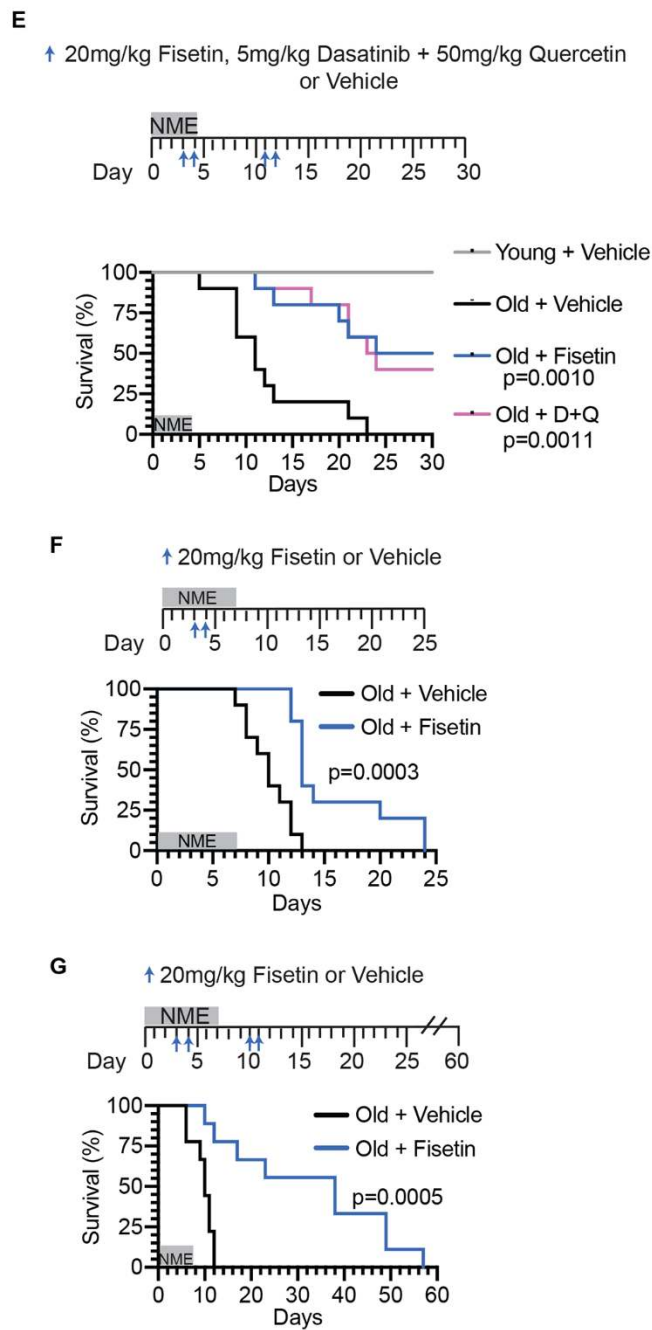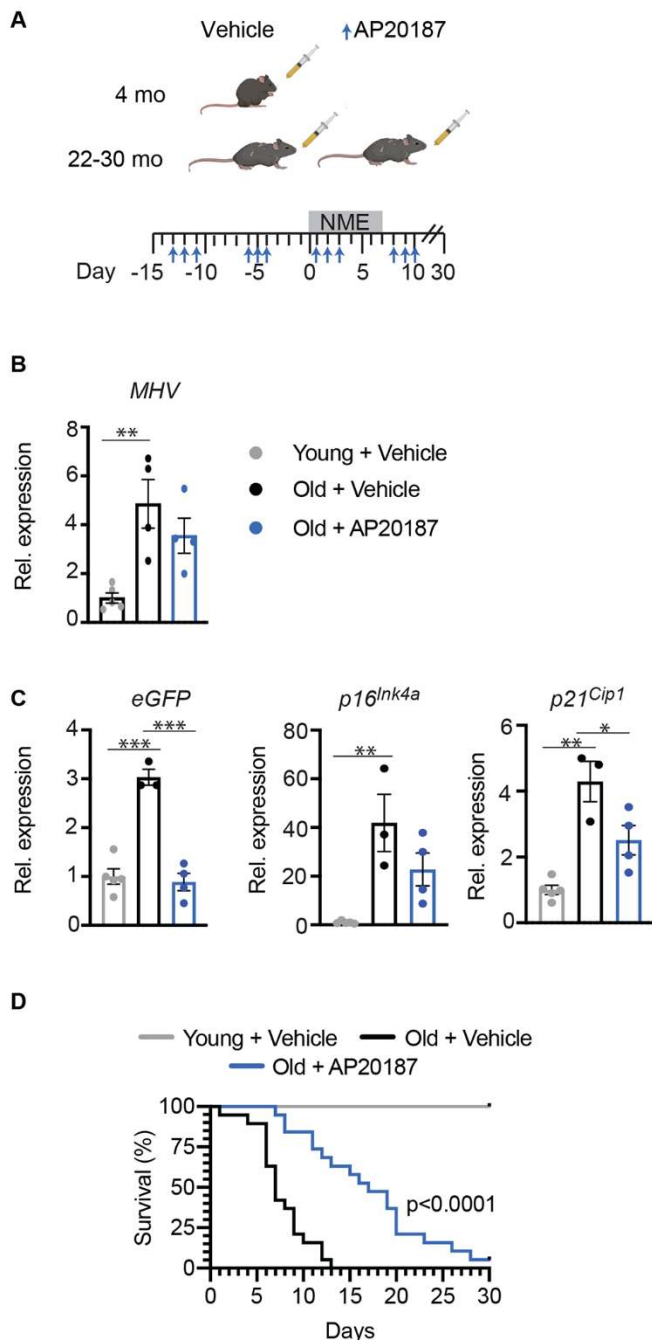
Fig. 5 (previous page). Pharmacologic and genetic ablation of SnC reduces mortality in old mice exposed to NME. (A) Schematic diagram of the experimental design for B-D. Young (4-month-old) and old (22-30-month-old) male and female *INK-ATTAC* mice were treated with vehicle or AP20187 (n = 10 young; n = 19 old + vehicle; n = 19 old + AP20187) to dimerize FKBP-caspase-8 fusion protein expressed in *p16^Ink4a+* cells to kill SnC selectively. AP20187 (10 mg/kg) or vehicle was administered i.p. daily for 3 days starting 2 weeks before initiating NME and ending 1 week after (3 days on and 4 days). NME was started on day 0 and lasted one week. Mice housed in SPF conditions were used as controls. Tissues were collected 7 days post-initiation of NME in another cohort of male animals for molecular analysis (n = 5 young ; n = 3-4 old + vehicle; n = 4 old + AP20187). (B) Quantification of MHV mRNA in fecal pellets isolated from individual mice. Means ± SEM, one-way ANOVA with Tukey's test. **$p < 0.01$. (C) Quantification of *eGFP* (a reporter of *p16^Ink4a* expression in the *INK-ATTAC* construct), *p16^Ink4a* and *p21^Cip1* mRNA in the kidney of mice in B. All expression data were normalized to young mice treated with vehicle. Means ± SEM, one-way ANOVA. *$p < 0.05$, **$p < 0.01$, ***$p < 0.001$. (D) Survival of male and female mice measured for 30 days post-initiation of NME. Log-rank [Mantel Cox] test. (E) Young (2-month-old, n = 5) and old (22-month-old, n = 10/group) female mice were exposed to NME bedding for 4 days. Beginning on day 3, mice were treated with 20 mg/kg Fisetin or 5 mg/kg Dasatinib plus 50 mg/kg Quercetin at days 3, 4, 11, and 12 by oral gavage, or with vehicle only. Survival was measured for 30 days post-initiation of NME. Log-rank [Mantel Cox] test. (F) Survival curves for 20-month-old WT female mice (n = 10/treatment group) treated with 20 mg/kg Fisetin or vehicle by oral gavage on days 3 and 4 following initiation of NME exposure. Log-rank [Mantel Cox] test. (G) Survival of 22-month-old WT female mice (n = 9/treatment group) treated with 20 mg/kg Fisetin or vehicle only by oral gavage at days 3, 4, 10, and 11 post-NME exposure monitored out to 60 days post. Log-rank [Mantel Cox] test.
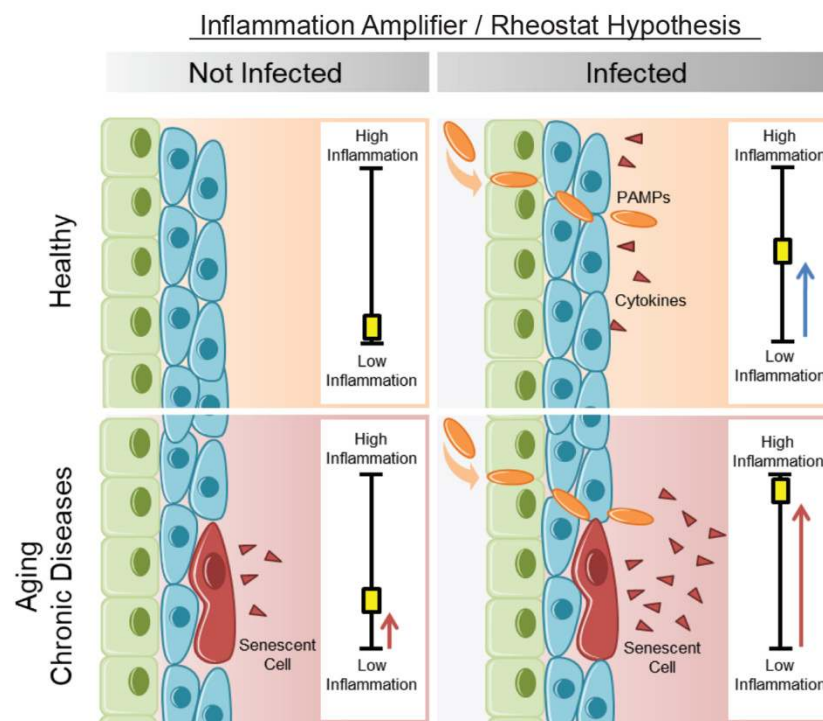

Fig. 6. SASP Amplifier/Rheostat Hypothesis. Schematic of the hypothesis generated from these data and tested herein. SnC amplified the response to PAMPs in vitro and in vivo, resulting in increased production of pro-inflammatory cytokines and chemokines. This could exacerbate acute systemic inflammatory responses and cytokine release by innate immune cells and amplify the spread of senescence. This model could explain the increased risk of cytokine storm during COVID-19 or other infections and adverse outcomes observed in the elderly or those with chronic conditions associated with an increased burden of SnC (obesity, diabetes, chronic lung or kidney disease, cardiovascular disease).